

Coexisting fast-slow dendritic traveling waves in a 3D-array electric field coupled neuronal network

Xile Wei(魏熙乐), Zeyu Ren(任泽宇), Meili Lu(卢梅丽), Yaqin Fan(樊亚琴), Siyuan Chang(常思远)

Citation: Chin. Phys. B, 2024, 33 (**6**): 068702. DOI: 10.1088/1674-1056/ad3228
Journal homepage: http://cpb.iphy.ac.cn; http://iopscience.iop.org/cpb

What follows is a list of articles you may be interested in

Effects of electric field on vibrational resonances in Hindmarsh-Rose neuronal systems for signal detection

Xiaoxia Li(李晓霞), Xiaopeng Xue(薛小鹏), Dongjie Liu(刘栋杰), Tianyi Yu(余天意), Qianqian He(何倩倩), and Guizhi Xu(徐桂芝)
Chin. Phys. B, 2023, 32 (**4**): 048701. DOI: 10.1088/1674-1056/ac9cc0

Simulation of the physical process of neural electromagnetic signal generation based on a simple but functional bionic Na^+ channel

Fan Wang(王帆), Jingjing Xu(徐晶晶), Yanbin Ge(葛彦斌), Shengyong Xu(许胜勇),Yanjun Fu(付琰军), Caiyu Shi(石蔡语), and Jianming Xue(薛建明)
Chin. Phys. B, 2022, 31 (**6**): 068701. DOI: 10.1088/1674-1056/ac3cac

Long range electromagnetic field nature of nerve signal propagation in myelinated axons

Qing-Wei Zhai(翟卿伟), Kelvin J A Ooi(黄健安), Sheng-Yong Xu(许胜勇), and C K Ong(翁宗经)
Chin. Phys. B, 2022, 31 (**3**): 038701. DOI: 10.1088/1674-1056/ac1e1a

An electromagnetic view of relay time in propagation of neural signals

Jing-Jing Xu(徐晶晶), San-Jin Xu(徐三津), Fan Wang(王帆), and Sheng-Yong Xu(许胜勇)
Chin. Phys. B, 2021, 30 (**2**): 028701. DOI: 10.1088/1674-1056/abc0d2

Closed-loop control of epileptiform activities in a neural population model using a proportional-derivative controller

Wang Jun-Song (王俊松), Wang Mei-Li (王美丽), Li Xiao-Li (李小俚), Ernst Niebur
Chin. Phys. B, 2015, 24 (**3**): 038701. DOI: 10.1088/1674-1056/24/3/038701

Coexisting fast–slow dendritic traveling waves in a 3D-array electric field coupled neuronal network

Xile Wei(魏熙乐)[1], Zeyu Ren(任泽宇)[1], Meili Lu(卢梅丽)[2], Yaqin Fan(樊亚琴)[1], and Siyuan Chang(常思远)[1,†]

[1] *The Tianjin Key Laboratory of Process Measurement and Control, School of Electrical and Information Engineering, Tianjin University, Tianjin* 300072, *China*

[2] *School of Information Technology Engineering, Tianjin University of Technology and Education, Tianjin* 300074, *China*

(Received 15 December 2023; revised manuscript received 5 March 2024; accepted manuscript online 11 March 2024)

Coexistence of fast and slow traveling waves without synaptic transmission has been found in hhhippocampal tissues, which is closely related to both normal brain activity and abnormal neural activity such as epileptic discharge. However, the propagation mechanism behind this coexistence phenomenon remains unclear. In this paper, a three-dimensional electric field coupled hippocampal neural network is established to investigate generation of coexisting spontaneous fast and slow traveling waves. This model captures two types of dendritic traveling waves propagating in both transverse and longitude directions: the N-methyl-D-aspartate (NMDA)-dependent wave with a speed of about 0.1 m/s and the Ca-dependent wave with a speed of about 0.009 m/s. These traveling waves are synaptic-independent and could be conducted only by the electric fields generated by neighboring neurons, which are basically consistent with the *in vitro* data measured experiments. It is also found that the slow Ca wave could trigger generation of fast NMDA waves in the propagation path of slow waves whereas fast NMDA waves cannot affect the propagation of slow Ca waves. These results suggest that dendritic Ca waves could acted as the source of the coexistence fast and slow waves. Furthermore, we also confirm the impact of cellular spacing heterogeneity on the onset of coexisting fast and slow waves. The local region with decreasing distances among neighbor neurons is more liable to promote the onset of spontaneous slow waves which, as sources, excite propagation of fast waves. These modeling studies provide possible biophysical mechanisms underlying the neural dynamics of spontaneous traveling waves in brain tissues.

Keywords: hippocampal network, epileptiform, dendritic oscillation, traveling wave, electric field coupling

PACS: 87.19.lq, 87.19.ll, 87.19.lj, 07.05.Tp **DOI:** 10.1088/1674-1056/ad3228

1. Introduction

Hippocampus plays a key role in memory and learning.[1] Abnormalities in the structure of hippocampus have been identified in patients with epilepsy.[2] Studies on electroencephalogram of epilepsy patients have shown that there are two types of traveling waves associated with hippocampus activity.[3] In the study of epilepsy, the speed of epileptic electrical signals propagating along the temporal and septal axes is always close to 0.1 m/s.[4] However, more in-depth experiments cannot be conducted on living human brain, which limits exploration of the mechanism of these traveling waves.[5]

Due to the limitations of *in vitro* experiments, many studies[6–8] used the isolated hippocampus tissue to reproduce this traveling wave and study its transmission mechanism. Measured *in vitro* in the hippocampus of rats, the wave propagation speed is about 0.1 m/s.[6] This measurement differs greatly from traditional synaptic transmission speed and gap junction. *In vitro* experiments using chemical antagonists and other means in several studies have shown that the transmission of epileptiform activity can be transmitted through a special mechanism without synapses.[7] The application of electrical stimulation to hippocampal CA1 neurons elicits dendritic oscillations within the hippocampus, providing evidence for the association between hippocampal dendritic oscillations and electric field coupling.[9] After blocking synapses, chemical synapses, electrical synapses and other mediators between neurons in rat hippocampus by using blockers (such as 4-aminopyridine (4-AP), which can block synapses between neurons), fast waves can still be found. It is well known that neuron excitation is accompanied by generation of transmembrane currents frequently, which induce spontaneous weak electric field within the neural network. Many studies have shown that the spontaneous weak electric field effect of neurons can affect the neuron's own excitation. This phenomenon has been confirmed by *in vitro* experiments of neural networks in both the hippocampus and the cortex.[8] Further experiments found that the fast oscillations are more likely to be related to spontaneous electric fields generated by hippocampal cells that activate neighboring neurons.[10] Subsequent experiments using dendritic N-methyl-D-aspartate (NMDA) channel antagonists (2-amino-5-phosphonovaleric acid, i.e., APV) have demonstrated that dendritic NMDA channels are involved in generation and propagation of this traveling wave.[11] All the above-mentioned tis-

†Corresponding author. E-mail: changsiyuan@tju.edu.cn

© 2024 Chinese Physical Society and IOP Publishing Ltd

sue experiments *in vitro* indicate the properties of this traveling wave in the hippocampus such that its generation and propagation depend on the dendritic NMDA channel and the electric field coupling of neurons acting as the propagation medium.

In further *in vitro* experiments on the hippocampus, a slow traveling wave with a slower propagation speed than the fast spike was first found to coexist with the fast traveling wave in the epileptic hippocampus.[12] The movement speed of this slow moving wave is only one tenth of that of fast waves, and it does not require NMDA receptors for propagation. The study used NMDA antagonists to demonstrate that the generation and propagation of this slow wave are independent of NMDA channels and the flow of calcium ions can be discovered in the generation and propagation process. Further experiments proved that the calcium channels of dendrites are involved in the neuronal periodic activity.[8] Another *in vitro* experiment has found that there is a suspected source of fast and slow waves coexisting in the hippocampus.[10] By using experimental methods such as photosensitive calcium protein reaction and Doppler effect, the continuous movement of wave source during the conduction process was determined.[6] A number of *in vitro* experiments have successfully reproduced this periodic oscillation in the hippocampus of rats.[13] The application of electrical stimulation to hippocampal CA1 neurons elicited dendritic oscillations within the hippocampus, providing evidence for the association between hippocampal dendritic oscillations and electric field coupling.[14] However, *in vitro* experiments cannot confirm the existence of a common source of fast and slow waves and can only be conducted based on this assumption, *in vitro* experiments are extremely demanding on the experimental environment and operation, and the measurement and processing of experimental results are faced with great difficulties, so it is impossible to deeply explore the mechanism of inducing dendrite waves. Traditional electrophysiological techniques obtain data through repetitive exploratory experiments, which are blind and have bioethical limitations. Therefore, it is necessary to establish a model to simulate the propagation process of fast and slow waves in the hippocampus.

In order to study neuronal activity in the hippocampus more conveniently, hippocampal neuronal models with different propagation modes have been established in many studies. The earliest studies utilized model simulations to test the role of electric fields in neural tissue.[15] By modeling and simulating the state changes of individual neurons during dendritic oscillations in the hippocampus, we have gained a better understanding of the process of dendritic oscillations.[16] The hippocampus was expanded from the middle to simulate the activity of neurons on a square array, which was propagated by two-way synapses between CA1–CA3 regions of the hippocampus.[9,10] This model provides a simplified idea to unfold the hippocampus before simulation but only considers the activity of synaptic transmission pyramidal neurons on one plane, and fails to use models to study electric field coupling and fast and slow waves. In subsequent research, a larger scale two-dimensional neural model was established to achieve bidirectional propagation of hippocampus in the model.[11] A two-compartment electric field coupled model was established to study the transmission of noise disturbance to hippocampus stimulation.[17] The simulation of the above-mentioned two models in the direction of electric field conduction is only unidirectional, which is different from the actual electric field conduction in the hippocampus. In epilepsy-like simulation, the propagation of fast and slow waves is bidirectional in the temporal septal direction. By establishing a 10×3 pyramidal neuron model, it is proved that electric field conduction can be conducted in the hippocampus at 0.1 m/s.[5] This model is small in structure, with only three layers of neurons. The propagation of nerve excitation in this model is one-direction, which can only verify the basic conclusions such as for the speed of the propagation. In our previous research, we established a two-compartment model to simulate the periodic activity of fast spikes and found that their propagation is closely related to the distance between hippocampal pyramidal neurons and NMDA channels.[8] Unfortunately, that two-compartment model cannot simultaneously arrange NMDA channels and calcium ion channels and was not comprehensive enough to study the coexistence of fast and slow waves. The present model simulates the bidirectional conduction of electric field in the longitudinal direction, ignoring the electric field propagation in the transverse axis. Although both the models provide a valuable foundation for our study, research of coexistence of fast and slow dendritic waves requires a more complete-structural and larger-scale model.

In this paper, we provide a novel three-compartment neuron array model based on our previous study. The model includes both NMDA channels and Ca^{2+} channels, as well as other neuronal structures, with a larger scale of 200×200 pyramidal neurons. Electric field coupling can occur in both longitude and traverse axes. This model enables us to explore the propagation mode and to identify common source of NMDA-dependent waves and Ca waves in the coexistence state. Using this model, we describe a new mechanism that dendritic Ca wave could act as the source of coexistence fast and slow waves. The model data validation verifies that the abnormal reduction of cell spacing reduces the threshold of stimulation required for generation of fast and slow waves, and increases the transmission speed of fast and slow waves. This type of hippocampus tissue isomerism is closely related to brain diseases such as epilepsy.

The rest of this paper is organized as follows: In Section 2 we introduce the basic structure and working method of

the model. In Section 3 we mainly present the data and conclusions obtained from model simulation in six sections. Subsections 3.1 and 3.2 show the bidirectional electric field conduction in the model on both transverse and longitude axes. In Subsections 3.3 and 3.4, we explore the roles of calcium ion channels and NMDA channels in the process of dendritic coexistence waves. In Subsection 3.5, it is verified that electric field coupling is the propagation medium of fast and slow coexisting waves. In Subsection 3.6, we explore the influence of cell spacing on the stimulation threshold and propagation speed of fast and slow waves, and simulate the relationship between local tissue spacing heterogeneity and epileptiform traits. Finally in Section 4, we presented a comprehensive analysis of the simulation results.

2. Materials and methods

2.1. Neuronal firing network

Based on the above-mentioned existing neuronal structure, we constructed the neuronal firing network. The object selected for simulation was a section of the rat hippocampus. The neuronal array simulates a region of approximately 350 μm(X) × 300 μm(Y) × 360 μm(Z) in the hippocampus, from the hippocampal septum to the temporal lobe for the longitudinal part of the neural network, and from area CA1 to area CA3 for the lateral part of the neural network (see Fig. 1).[18] The neuronal network is located in an approximate rectangular space with the x-axis direction representing the longitudinal direction and the y-axis direction representing the transverse direction, as shown in Fig. 1. The z-axis represents the stacking of multiple layers of neurons (see Fig. 1), and to simplify the model, we introduced a stacking factor (SF) to replace the mutual influence between different layers of neuronal networks. Therefore, the object of our study is a single-layer 200(X-axis) × 200(Y-axis) neuron matrix (see Fig. 1).[19]

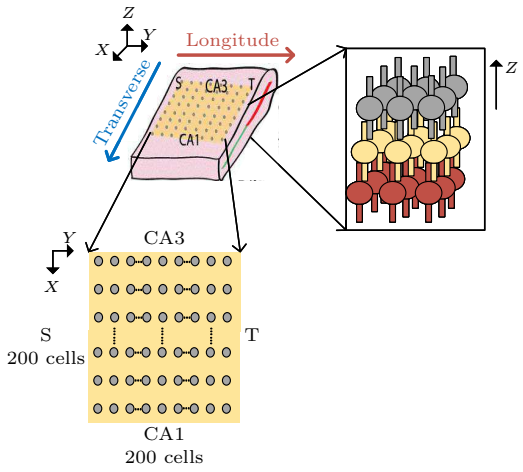


Fig. 1. Transmittance for the eigenvalues of the cavity including the BP and BC, plotted as a function of $\Delta\varphi$ for the case of $\beta = 45°$.

2.2. Electric field coupling

When an action potential occurs at the dendrite, current flows out the soma and in at the dendrites, creating a local current loop. This loop will in turn depolarize the adjacent neuron that was originally at rest and modulate its electrical activity (see Fig. 2). The conduction of electric fields is isotropic, whereas it is not realistic to fully achieve electric field conduction in all directions in the model. Researchers have showed that the multidirectional electric field conduction of neurons mainly follows these two vertical directions.[20] To verify that the neuronal spontaneous electric field is able to induce the slow oscillations found in *in vitro* experiments, the model assumes that the neuronal electric field is conducted in both the X and Y directions and that the electric field is bidirectional in each axis. The calculation of the neuronal electric field follows exactly the laws of electrical correlation.[21] Since each neuronal cell can be approximated as a point current source, according to Ohm's law and the potential calculation formula, the potential at any point in the electric field it forms can be given such that ρ is the equivalent resistance between the point and the current source, I is the current source strength, and r is the linear distance between the point and the center of the current source. Based on the electric field coupling relationship between cells (Fig. 3) with Eq. (1), we can calculate all extracellular potential to any compartment in the neuronal network as follows:

$$\phi = \frac{q}{4\pi\varepsilon_0 r} = \frac{I\rho}{4\pi r}, \tag{1}$$

$$V_{(k,l)_e_z} = \mathrm{SF} \times \frac{\rho}{4\pi} \sum_{(i,j)} \left(\frac{I_{(i,j)_\mathrm{tran}_d}}{r_{(i,j)_d \to (k,l)_z)}} + \frac{I_{(i,j)_\mathrm{tran}_s}}{r_{(i,j)_s \to (k,l)_z)}} \right), \quad (z = d, s), \tag{2}$$

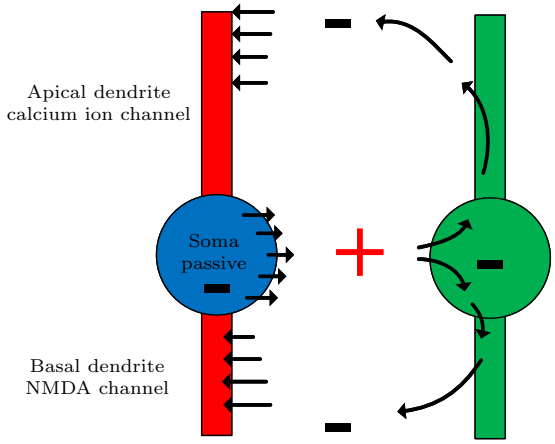


Fig. 2. Graphical demonstration of electrical field effect for cell to cell interaction. In ion flow, pyramidal neurons can be regarded as an independent current source, generating an electric field centered around the current source.

In Eq. (2), $V_{(k,l)_e_z}$ is the extracellular potential inserted at target compartment z of the target cell(k,l), $I_{(i,j)_\text{tran}_d}$ is the transmembrane current of two compartments in source cell$_{(i,j)}$ located at distances $r_{(i,j)_d\to(k,l)_z}$ and $r_{(i,j)_s\to(k,l)_z)}$ from the target compartment z.[22] To better observe the propagation of fast spikes and slow waves in the model, simulated electrodes were applied to the exterior of the hippocampus to measure the traveling wave data in the model (see Fig. 4).

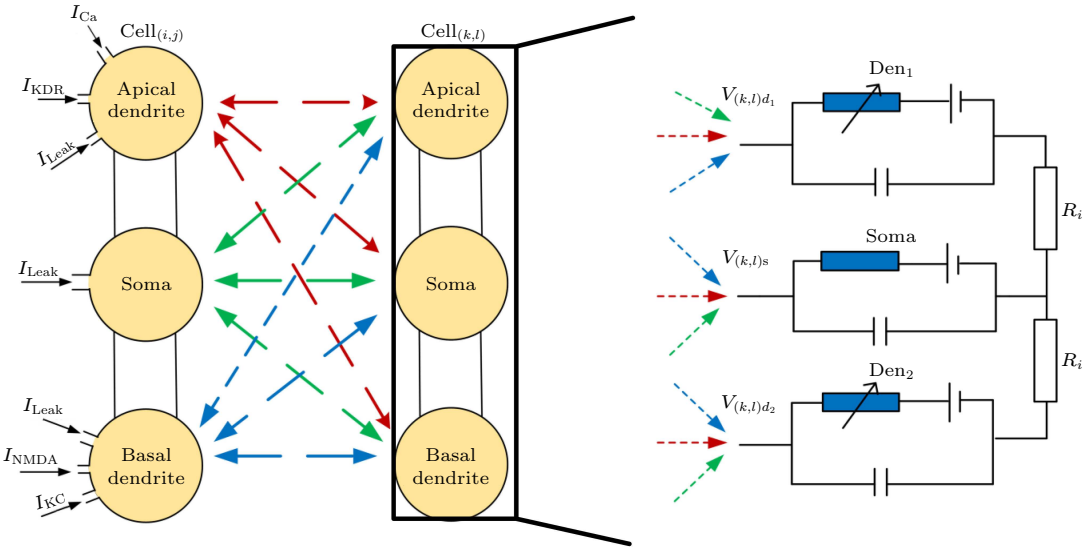


Fig. 3. Neuron model ion channel distribution and bidirectional electric field coupling (left), as well as the circuit model of conical neurons used in simulation (right).

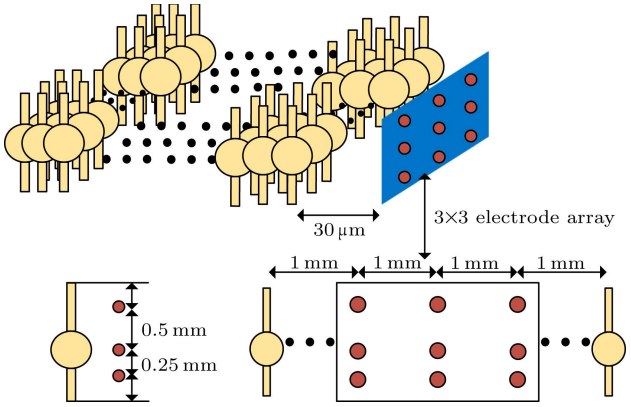


Fig. 4. A virtual 3×3 electrode array is placed at 30 μm away from the neuronal array. The electrodes measure potential information in the apical dendritic layer, the somatic layer and the bottom dendritic layer, respectively.

2.3. Model operation method

The structure of the model consists of weight matrix, coordinates matrix, state variables matrix, etc. Based on the weight matrix, coordinate matrix and initial extracellular stimulus, the initial state matrix of the neuron is obtained. The state matrix contains neuronal transmembrane potential, calcium channel coefficients, etc. To describe the simultaneous conduction of the spontaneous electric field in the X and Y axes for simplifying the calculation, we take into account the superposition effect of the electric field. The model is used to calculate the electric field in both directions separately, superimposing them together and including them in the iteration of the state matrix. The single step of state iteration is 0.1 ms, and the total iteration time is 5000 ms. The model assumes that the iteration time exceeds half of the total period before reverse conduction begins, and the updated weight matrix is used to simulate bidirectional conduction. The data are processed separately outside the model, and the neuronal state matrix at each time point allows us to observe the electric field conduction of the same neuron at different times, in the same way as data from *in vitro* experiments.[9]

2.4. Single neuron structure

2.4.1. Cell scale

In the hippocampal neural network model, each hippocampal pyramidal neuron cell contains three compartments, one of which, as the cell body of the neuron, contains only one leakage channel and is in a passive state in the whole oscillation process. The other two compartments are the apical dendrites and the basal dendrites. We used Matlab simulation to conduct mathematical modeling of this neuron structure (see Fig. 3). This model can be used to test the slow oscillations of pyramidal neurons under various experimental conditions *in vitro*. In the model, the spacing between adjacent neuron centers was 15.8 μm, which mimics the diameter of pyramidal neuron cells under normal physiological conditions. The cell radius and cell spacing of pyramidal neurons are affected by concentration in the environment. Low calcium environment induces cell swelling, and the spacing of adjacent cells decreases accordingly.[23] The effect of concentration on slow wave propagation was tested by changing the radius of cone

cells in the model.

2.4.2. NMDA channel

NMDA receptors are widely distributed in the dendritic portion of pyramidal neurons. To scientifically describe the activity of neuronal arrays, we included NMDA receptors in the neuronal model, located on the parietal dendrites. Magnesium is a negative allosteric at NMDA glutamate receptors. The extracellular concentration of magnesium ions determines the degree of opening and closing of NMDA channels, and we take the coefficient B to express the effect of magnesium ion concentration in the extracellular environment on the conductance of NMDA channels.[24] This gating function is

$$B = \frac{1}{1+\exp(-k_{\mathrm{B}}V_{\mathrm{md}})\frac{[\mathrm{Mg}^{2+}]}{M_0}}. \tag{3}$$

2.4.3. Leaky channel

Since somatic cells are passive interneurons, there is only one channel for leakage current on the cytosolic neurons. Such a design can also test the spike found in *in vitro* experiments that do not require NMDA channels.

2.4.4. Ca^{2+} channel

Calcium channels are located on the cell membrane and allow calcium ions to enter the neuron upon opening.[25] The influx of calcium triggers a variety of neuronal processes such as neurotransmitter release, gene transcription, and plasticity mechanisms that enable learning and memory. Voltage-gated calcium channels open in response to membrane depolarization caused by neuronal excitation. Calcium channels have also been shown to play a key role during fast and slow-wave conduction in hippocampal neurons, which in models are located on the apical dendrites of neurons. To better characterize the function of calcium channels, relevant potassium channels were also introduced into the model. The inverse relationship between potassium and calcium channels establishes a feedback loop that underlies action potential. In the model, this operation can be simulated by the conductance value of the potassium channel $g_{m_{\mathrm{kc}}}$.

2.4.5. Other fixed parameters of neurons

In order to be comparable with the *in vitro* experimental conditions, we designed some neuronal parameters as follows: somatic membrane resistance $R_{\mathrm{ms}} = 680\ \Omega/\mathrm{cm}^2$, the membrane resistance of parietal dendrites and bottom dendrites are the same, $R_{\mathrm{md1}} = R_{\mathrm{md1}} = 780\ \Omega/\mathrm{cm}^2$, intracellular resistance $R_{\mathrm{i}} = 530\ \Omega/\mathrm{cm}^2$, extracellular resistance $R_{\mathrm{i}} = 530\ \Omega/\mathrm{cm}^2$. Dendrites and somatic membrane capacitance are equal, $C_{\mathrm{md}} = C_{\mathrm{ms}} = 1\ \mu\mathrm{F/cm}^2$. The other fixed parameters are listed in Table 1.

Table 1. The electronic parameters in the computational model.

Parameter	Symbol	Value
Somatic membrane resistance	R_{ms}	680 Ω/cm^2
Dendritic membrane resistance	$R_{\mathrm{md1}}R_{\mathrm{md1}}$	780 Ω/cm^2
Intracellular resistance	R_{i}	530 Ω/cm^2
Extracellular resistance	R_{e}	300 Ω/cm^2
Dendrites membrane capacitance	C_{md}	1 μF/cm^2
Somatic membrane capacitance	C_{ms}	1 μF/cm^2

2.4.6. Hudgkin–Huxley model

The cell membrane model used in the model is the Hodgkin–Huxley model, which is closer to the physiological, electrochemical properties of real neurons (see Fig. 3). According to the gating function of this model, the ion current values of each ion channel of the neuron are obtained, and then we can obtain the transmembrane potential by the following equation:

$$\frac{\mathrm{d}V_{\mathrm{md1}}}{\mathrm{d}t} = \frac{1}{C_{\mathrm{md}}}(-I_{d1_\mathrm{NMDA}} - I_{s_d1} - I_{d1_\mathrm{Leak}} - I_{d1_\mathrm{stim}} - I_{d1_d2} - I_{\mathrm{KDR}}), \tag{4}$$

$$\frac{\mathrm{d}V_{\mathrm{ms}}}{\mathrm{d}t} = \frac{1}{C_{\mathrm{ms}}}(-I_{d1_s} - I_{s_\mathrm{Leak}} - I_{s_\mathrm{stim}} - I_{d2_s}), \tag{5}$$

$$\frac{\mathrm{d}V_{\mathrm{md2}}}{\mathrm{d}t} = \frac{1}{C_{\mathrm{md}}}(-I_{d2_\mathrm{Leak}} - I_{d2_\mathrm{Ca}} - I_{d2_\mathrm{KC}} - I_{d2_\mathrm{KAHP}} - I_{d2_\mathrm{stim}} - I_{s_d2}), \tag{6}$$

$$I_{\mathrm{NMDA}} = -g_{\mathrm{NMDA}}B(V_{\mathrm{md1}} - E_{\mathrm{NMDA}}), \tag{7}$$

$$I_{\mathrm{KDR}} = -g_{m_\mathrm{KDR}}\eta^4(V_{\mathrm{md1}} - E_{\mathrm{K}}), \tag{8}$$

$$I_{\mathrm{Leak}} = -g_{m_\mathrm{Leak}}B(V_{\mathrm{m}} - E_{\mathrm{Leak}}), \tag{9}$$

$$I_{\mathrm{KAHP}} = -g_{m_\mathrm{KAHP}}q(V_{\mathrm{m}} - E_{\mathrm{Leak}}), \tag{10}$$

$$I_{\mathrm{Ca}} = -g_{m_\mathrm{Ca}}m_{\mathrm{Ca}}^2h_{\mathrm{Ca}}(V_{\mathrm{md2}} - E_{\mathrm{Ca}}). \tag{11}$$

Some fixed conductance and potential in the model are listed in Table 2.[22]

Table 2. Some fixed conductance and potentials in the equation.

Parameter	Symbol	Value
NMDA channel conductance	g_{NMDA}	6.5 ms/cm^2
Potassium ion channel conductance	g_{KDR}	200 ms/cm^2
Somatic membrane leak conductance	g_{msLeak}	1.4706 ms/cm^2
Dendritic membrane leak conductance	g_{mdLeak}	0.0292 ms/cm^2
Resting potential of NMDA channels	E_{NMDA}	0 V
Resting potential of ion channel conductance	E_{K}	−60 mV
Resting potential of leaking channel conductance	E_{Leak}	−58 mV
Resting potential of calcium ion channels	E_{Ca}	10 mV

The dynamics of gate variable η for I_{KDR} and m_{Ca}, h_{Ca} for I_{Ca} are described by

$$\frac{\mathrm{d}\eta}{\mathrm{d}t} = \alpha - \eta(\alpha+\beta), \tag{12}$$

$$m_{\mathrm{Ca}} = \frac{m_{\mathrm{CaH}}}{\tau_{\mathrm{mCaH}}}, \tag{13}$$

$$h_{\mathrm{Ca}} = \frac{h_{\mathrm{CaH}}}{\tau_{\mathrm{hCaH}}}, \tag{14}$$

with the variable rate functions

$$\alpha = \frac{0.00049V_{\rm md}}{1-\exp(-\frac{V_{\rm md}}{25})}, \tag{15}$$

$$\beta = \frac{0.00008(V_{\rm md}-10)}{\exp(-\frac{V_{\rm md}-10}{10}-1.0)}, \tag{16}$$

$$m_{\rm CaH} = \frac{1}{1+\exp(-\frac{V_{\rm md}+20}{16})}, \tag{17}$$

$$h_{\rm CaH} = \frac{1}{1+\exp(\frac{V_{\rm md}+40}{7})}. \tag{18}$$

3. Results

3.1. Simulation of bidirectional electric field conduction

3.1.1. Slow periodic waves propagating non-synaptically in the model

Before proceeding with the simulation of the relevant experiments, we first verify that the model is able to simulate fast and slow waves in the hippocampal phenomenon while cutting off other neuronal connections.[18]

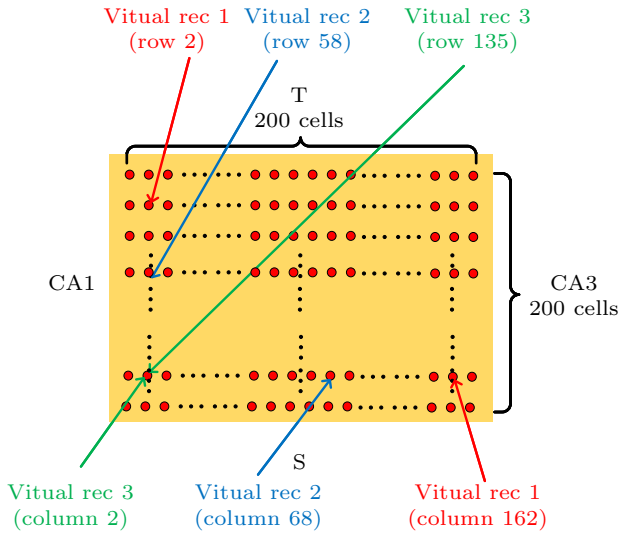


Fig. 5. Virtual electrode measurement membrane potential in three different neurons from the same column and row in two directions in an array of hippocampal neurons.

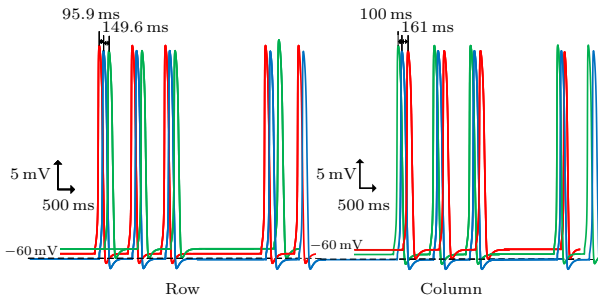


Fig. 6. Slow waves measured by three virtual electrodes in the longitude and traverse directions and the time interval between them.

We adjusted all channel conductance of the model to normal values and simulated the maintenance of extracellular magnesium and calcium ion concentrations at equilibrium. In the simulated hippocampal sections, we inserted virtual 'electrodes' to record the membrane potential changes of the neuronal cells in two directions during the simulation (see Fig. 5). With three simulated electrodes in the same row and column in both of the traverse and longitudinal directions, we can estimate the speed of propagation (see Fig. 6). Due to the random nature of the initial state of the model, the propagation speed is subject to error, and we obtain multiple sets of data from multiple simulations to estimate the propagation speed statistically.

The results obtained from the simulation show that the model can generate and propagate slow periodic waves normally under the initial conditions, and the slow wave is conducted in traverse and longitude directions at an approximately constant speed. Based on the distance between the measured neuron cells and the time of wave peak arrival, the speed of slow waves in the simulation can be roughly calculated.[19] After several experiments, the slow periodic propagation speed was statistically obtained to be 0.009 ± 0.003 m/s.

3.1.2. Fast traveling spikes propagating spontaneously in the model

Using the same method while observing slow waves, we observed spike continuous discharges in neuronal cells. According to the relevant parameters of the *in vitro* experiment, the conductivity value of the NDMA channel was set. The results obtained from the simulation show that the model can generate and propagate fast spikes spontaneously normally under the initial conditions. Within a period, the propagation of

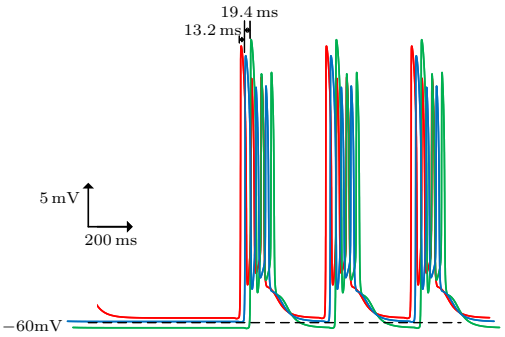


Fig. 7. Fast spikes measured by three virtual electrodes and the time interval between them.

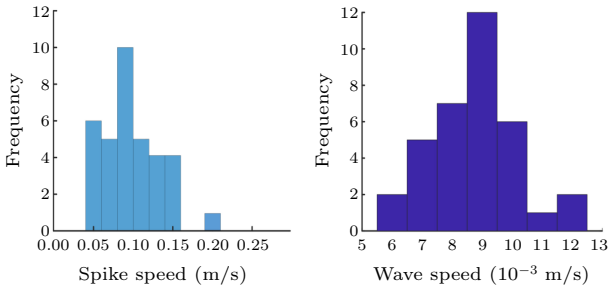


Fig. 8. To exclude the effect of experimental error, 35 replicate tests were performed. The speed histogram displays the statistical speed of fast spikes and slow waves.

fast waves takes on the form of clustered spikes (see Fig. 7). The fast wave propagation speed was statistically obtained to be 0.1 ± 0.02 m/s (see Fig. 8).

3.1.3. Coexsistence of fast spikes and slow waves in hippocampal

Fast spikes and slow-wave propagation can be found simultaneously in the model. To better observe the propagation of fast spikes and slow waves in the model, simulated electrodes were applied to the exterior of the hippocampus to measure the traveling wave data in the model. The neural electric field of the hippocampus measured by virtual *in vitro* electrodes. The maximum electric field in the hippocampus was 11 mV/mm, and the peak appeared at a time that basically coincided with the firing spikes of neuronal cells (see Fig. 9). The fast spikes were filtered out by a high-pass filter, and the fast spikes at different locations maintained essentially the same frequency and speed. Similarly, using a low-pass filter, slow wave data at different locations can be obtained (see Fig. 10), again with similar frequencies and propagation velocities. To further compare the reproduction of the model for the *in vitro* experiments, multiple repetitions of the experiment varying the parameters were performed. By varying the stacking factor (SF) of neuronal cells, multiple sets of experimental data were obtained (see Fig. 11). It can be found that when the cell stacking factor increases, the neuronal cell field strength increases continuously to about 21 ± 0.5 mV/mm, the field strength increase becomes smaller and the field strength remains basically constant.[26] The distance between neurons (D_{cc}) decreases to 2 mm and 3 mm, respectively, under constant neuronal stacking factor. The electric field intensity inside neurons significantly increases. At the same time, the measured speed of fast- and slow-wave propagations also increases (Fig. 11). If the stacking factor of the cells is too low, no wave will be generated in the simulated neural network. The frequency of continuous fast spikes fluctuated between 0.5 Hz and 1.1 Hz, with an average value of 0.72 ± 0.25 Hz, and the speed ranged from 0.04 m/s to 0.2 m/s, with an average value of 0.12 ± 0.04 m/s. The ratio of the speed between fast and slow waves during propagation is in the range of 9–11, with an average value of 9 ± 1.2, and the ratio of amplitude is in the range of 7–13, with an average value of 10 ± 1.5. The traveling waves obtained from the simulations have similarity to the data obtained in the experiments.[27] Simulations are basically consistent with the *in vitro* experimental data. However, the error of model simulation for the same data is smaller than that of *in vitro* experiments.

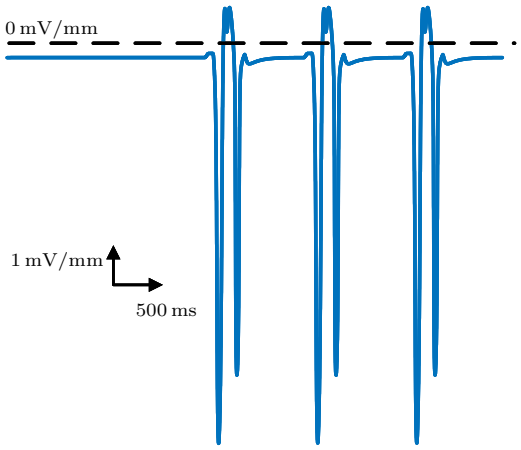


Fig. 9. The neural electric field of the hippocampus measured by virtual *in vitro* electrodes.

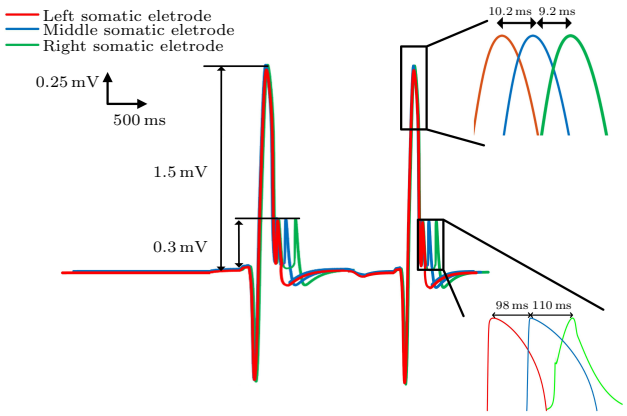


Fig. 10. Local electric potential recorded at a medium virtual electrode close to the somatic. The simulated spikes can demonstrate the coexistence of fast wave oscillations with slow wave propagation. By high and low pass filtering of the data measured at the electrodes at different locations, the wave speed and amplitude of the fast and slow waves can be measured.

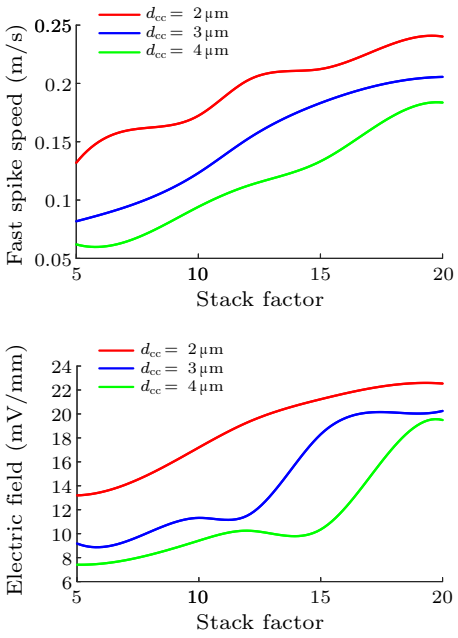


Fig. 11. The relationship between the fast spoke speed and extracellular electric field and the cell spacing (d_{cc}) and stacking factor (SF).

3.2. The source of the fast spike moving in a train of spikes

Although the propagation direction of slow waves is basically fixed, in the simulation, it was found that the propagation direction of fast spikes is not the same as slow waves. Because of the high propagation speed of fast waves, it is hard to determine the position change of wave source only by the membrane potential of several neurons. In the model simulation, the membrane potential heatmap can help us better judge the change of the fast spike source. Utilizing the recorded membrane potential data from a single nerve cell, we choose the membrane potential distribution across an entire neuronal array in a specific spike train.

Subsequently, a heat map representing the neuronal membrane potential is generated to reconstruct the origin and direction of propagation for these spike events. The membrane potential heatmap in this study is derived from a segment of the membrane potential within the neuronal array at coordinates (100, 100) of the pyramidal neurons. It captures six moments within the array corresponding to three instances of fast peaks and troughs. By analyzing the changes in the membrane potential before and after the peaks, we attempted to determine the source location of the fast wave. It can be observed that prior to the first peak in the pyramidal neuron, action potentials are first generated in neurons on the septal side. Locally activated dendrites discharge, and under the influence of electric field coupling, activate nearby dendrites in the region. The fast wave propagates to the target neuron, resulting in a peak. It can be observed that in this instance, the fast wave propagates from the septal to the temporal lobe. In the next moment, we captured the generation of new action potentials in the middle of the neuronal array, spreading outward in all directions, as observed in the membrane potential heatmap. The source of this fast wave oscillation was located in the middle of the neuronal array. The last two heatmaps depict the process of the final excitation of the pyramidal neuron at coordinates (100, 100). The fast wave initially appeared in the lower right corner of the neuronal array (i.e., the temporal lobe side). Furthermore, the sequence of spike trains recorded by extracellular electrodes in the subsequent figure provides additional evidence, supporting the conclusion that the source of the fast wave underwent a movement from the septal to the temporal lobe. During this movement, one or multiple discharge events also occurred (see Fig. 12). This particular phenomenon has also been observed in *in vitro* experimental settings,[6] with the model demonstrating the capacity for accurate replication.

One potential explanation for this occurrence is that the wave source undergoes a continuous movement, with the source's velocity being considerably lower than that of the wave propagation. Through the examination of the membrane potential's thermodynamic diagram, a distinct pattern of wave source movement can be discerned. The simulation data unequivocally supports the notion that the wave source's movement is not a fleeting event, but rather a gradual process that unfolds in tandem with the wave propagation (Fig. 12). The three electrodes recorded the arrival time of three peaks in a peak queue, indicating that the order of wave peak arrival is not fixed.

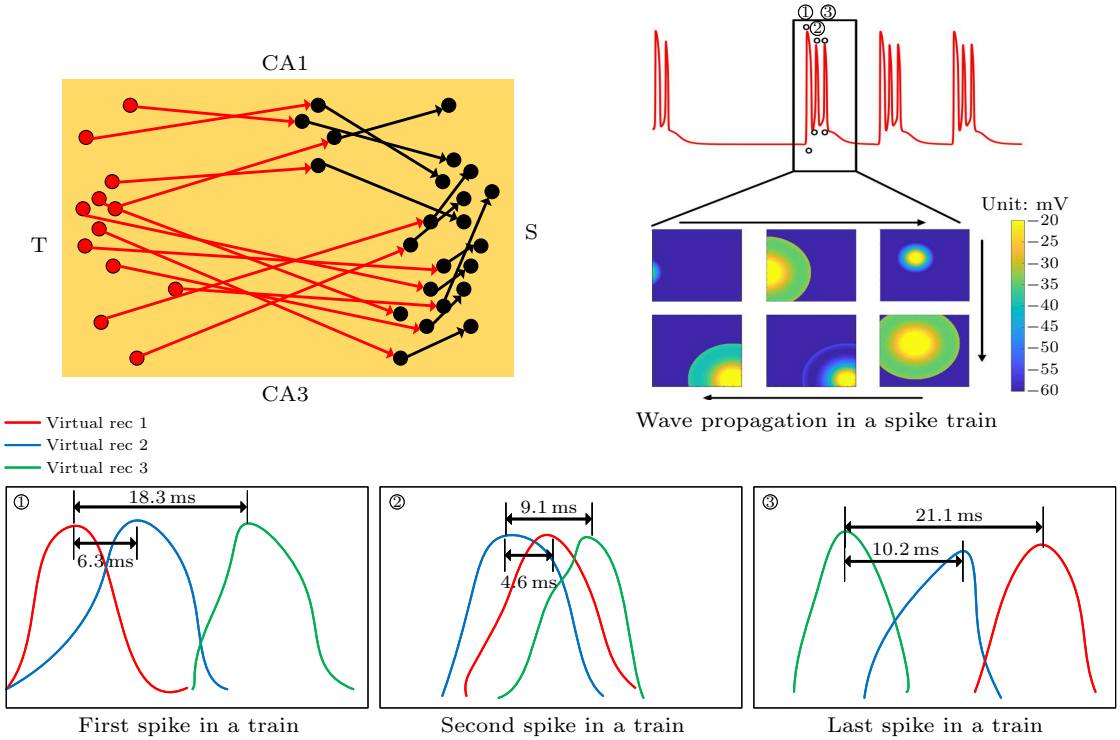


Fig. 12. The location of the wave source for the multiple spike queue (35 events) (top left). It can be found that the change in the position of the wave sources occurs under the current simulation conditions.

3.3. The function of NMDA channels in propagation

In our study, we demonstrated with model simulations that NMDA waves play a key role in the generation of fast and slow waves of dendrites in hippocampus.[28] In this subsection we explore the role played by NMDA channels in generation of slow waves. The first method is to dynamically change the conductance of the NMDA channel in conduction and to observe the effect of this dynamic change on the generation of slow oscillations. Neurophysiological studies have shown that NMDA channels are populated with magnesium ions that block the passage of other ions to stifle the generation of neural excitation (see Fig. 13). If the extracellular magnesium ion concentration rises, it affects the degree of opening of the NMDA channel with the gating function shown in Eq. (1). Therefore, the second method is to change the extracellular magnesium ion concentration and to explore the role of the degree of opening and closing of NMDA channels on slow-wave propagation.

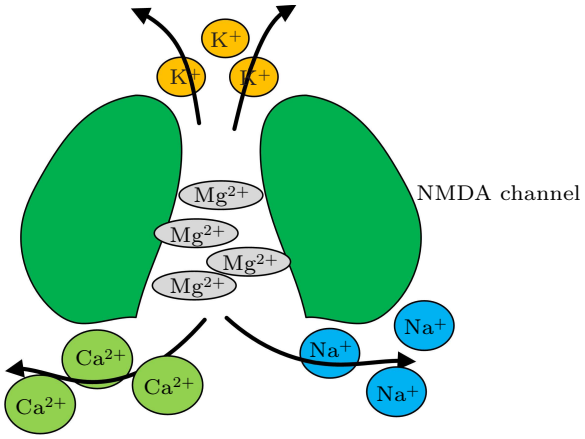


Fig. 13. NMDA receptors possessing a magnesium ion block mechanism.

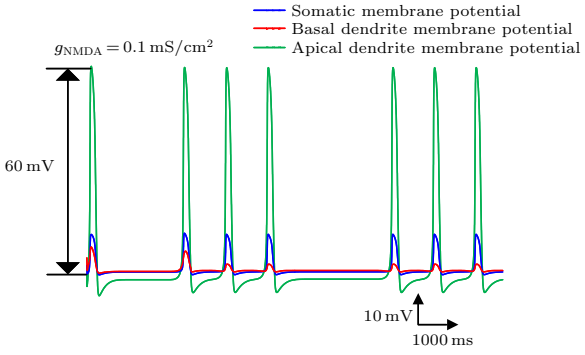


Fig. 14. Method 1: after removing the NMDA channel wave (NMDA conductivity is reduced to 0.5 mS/cm^2), the slow wave generation of calcium ions is not affected.

We set the conductivity of the NMDA channel to a lower physiological value. Try to limit the role of NMDA channel in membrane potential through low conductivity [Eq. (3)]. In the model simulations, no clear change in the slow wave propagation process was observed (Fig. 14), where fast spikes no longer generated. Calcium waves generated by calcium channels also disappear after a spike and cannot propagate independently of NMDA waves. For the tests of method 2, we set the extracellular magnesium ion concentration at 0.5 mM and 2 mM, respectively, to compare the propagation produced with the normal concentration of 1 mM used in the *in vitro* experiments. Decreasing the concentration of Mg^{2+} would increase the ion inflow of NMDA channels, raising the resting potential of NMDA channels and greatly increasing the difficulty of spike generation. The NMDA channel activity decreases after increasing the magnesium ion concentration. The peaks of NMDA spike and firing frequency decrease (see Fig. 15). Both the above model experiments demonstrate the critical role of NMDA channels in fast spikes activity. However, calcium wave production is not affected by changes of NMDA channel activity in the experiments, which is consistent with the results of method 1.

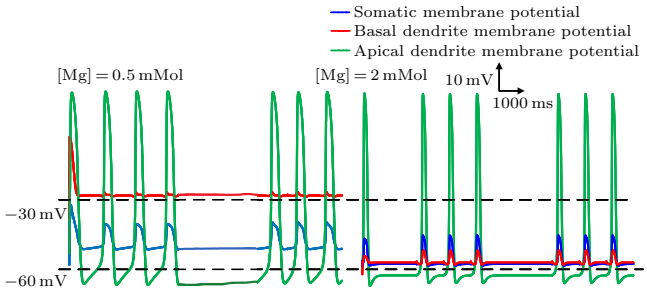


Fig. 15. Method 2: after adjusting the concentration of extracellular magnesium ions, the NMDA peak disappears and the generation of slow waves of calcium ions is not affected.

3.4. The function of calcium ion channels in propagation

Calcium channels serve as crucial ion channels that significantly contribute to the modulation of various aspects of neuronal activity.[29] These channels are implicated in the initiation and propagation of action potentials, as well as in synaptic plasticity and the regulation of neurotransmitter release. Moreover, they have been identified as playing a pivotal role in the generation of slow wave activity and modulating the activity of other ion channels, such as NMDA channels. Compared to *in vitro* experiments, computational models enable the fine-tuned regulation of calcium channel opening and closing, providing a clearer visualization of the impact of these channels on slow-wave conduction. Calcium channel conductance may range from 0.1 to 56. The influence of calcium channels on NMDA wave and slow wave propagation can be ascertained by observing the alterations in membrane potential within various compartments of the same cell, as conductance values span different ranges (see Fig. 16). Changes of hippocampal neuronal cell membrane potential in calcium channel conductance are observed. When calcium channel activity is overactive, fast spikes and slow waves are no longer generated after a continuous spike train. Changes of membrane potential during fast and slow wave propagation will affect hip-

pocampal neuron cells under normal conditions. When reducing the calcium channel conductance to 0.5 times the normal value, the slow waves generated by calcium channels are not affected, but the NMDA spike train excitability is reduced, and the original three spikes in a train are reduced to two spikes. When decreasing the calcium channel conductance of neuronal cells to 0.1 ms/cm^2, the neuronal fast- and slow-wave propagations will completely disappear.

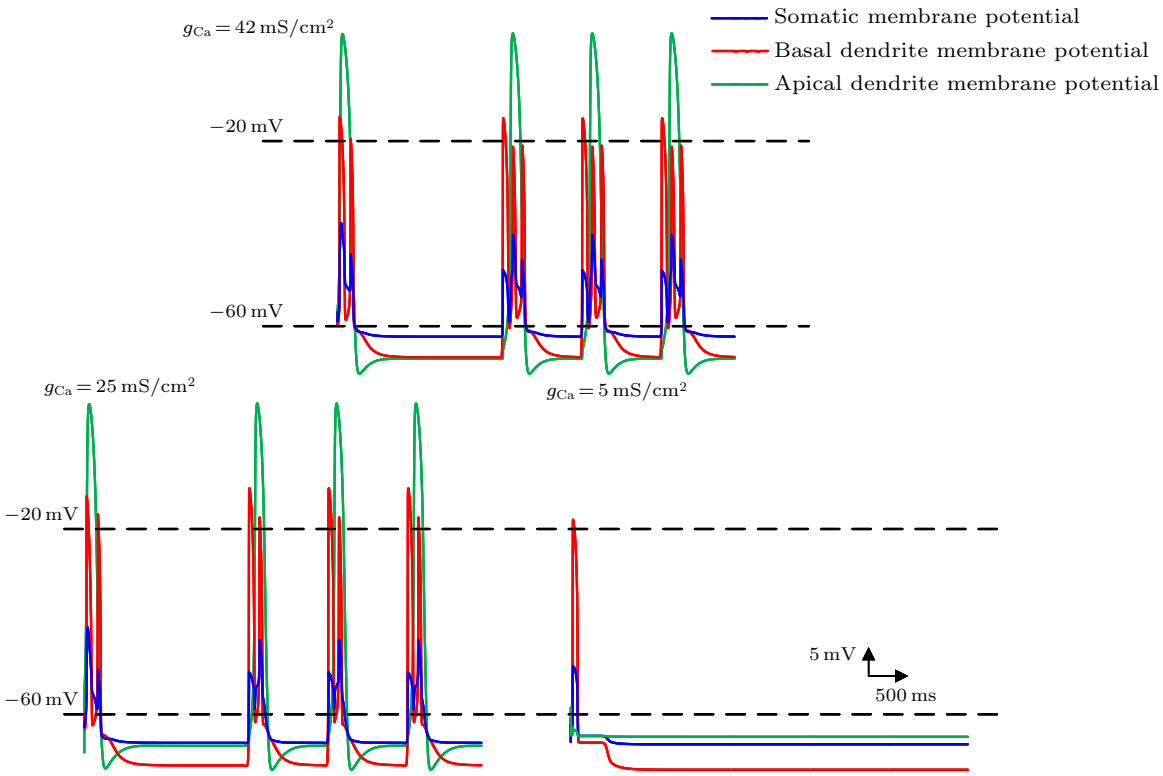


Fig. 16. The generation of fast and slow waves in pyramidal neurons during changes in calcium ion channels.

In scenarios where either calcium channels are absent or they exhibit minimal opening, neuronal electrical field conduction is entirely obstructed. As calcium channels progressively open, slow-wave conduction is observed within the neuronal array. However, NMDA wave excitability remains low, and the frequency of spike occurrences diminishes. It is only upon restoring the degree of calcium channel opening that NMDA excitability reverts to normal levels. These simulations demonstrate the critical role of calcium channels for slow-wave conduction. This role is reflected in the direct involvement of calcium channels not only in the formation of slow waves, but also in their modulation of NMDA channels.

3.5. Electric field conduction plays a key role in slow conduction

In order to further investigate the influence of electric field effects on slow-wave propagation, relevant electric field experiments were conducted using the model. According to Eq. (17), the intensity of electric field induction between neurons is inversely related to the distance between them. *In vitro* experiments often involve physically severing the rat hippocampus to examine the dependence of slow wave propagation on the physical spacing between neurons.[6]

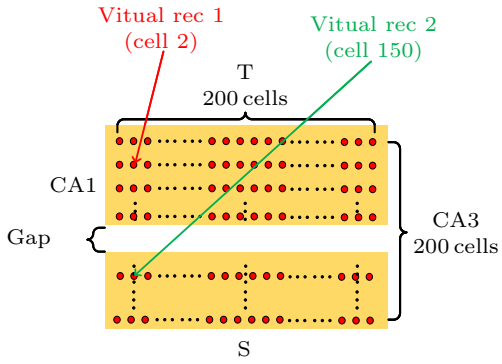


Fig. 17. Physical severance performed between the two columns of cells and between rows 100 and 101 in the hippocampus. The size of the gap gradually increases, and the changes of membrane potential of neurons before and after the gap are observed.

Model simulations can conveniently replicate *in vitro* experiments by adjusting the distance between adjacent neuronal cells. In the model, the center of the neuronal cell array (between columns 100 and 101) is severed, and the distance is set to 2000 times the adjacent cell spacing (see Fig. 17). Simulated electrodes are positioned at one neuronal cell before and one after the break to monitor excitation conduction (see Fig. 18). The membrane potential changes of the cells in front of the gap can be observed. Some NMDA spikes in spike train are missing, and it is inferred from previous simulations that

the wave source located in the hippocampal septal lobe could not propagate through the gap. For the cell membrane potential after the gap, no electric field propagation occurs in neurons, which remains at resting potential.

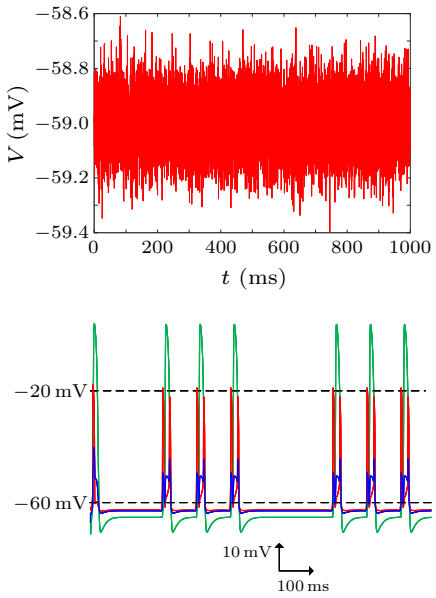


Fig. 18. Neuron membrane potential before and after the gap with 2000-cell spacing (left: after the gap, right: before the gap).

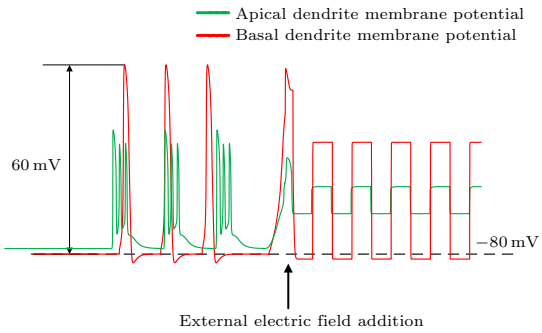


Fig. 19. Neuron membrane potential before and after the gap with 2000 cell spacing (left: after the gap right: before the gap).

The results show that excitation cannot be conducted in both directions across the break. These experiments suggest that increasing physical distances can hinder neuronal excitation conduction, and this phenomenon is explained in terms of electric field conduction. Moreover, electric field conduction is proposed as the mediator of slow-wave conduction through the applied electric field in the model. When an electric field is introduced to the neuronal array from the septum to the temporal lobe, and the reverse electric field is continuously strengthened.

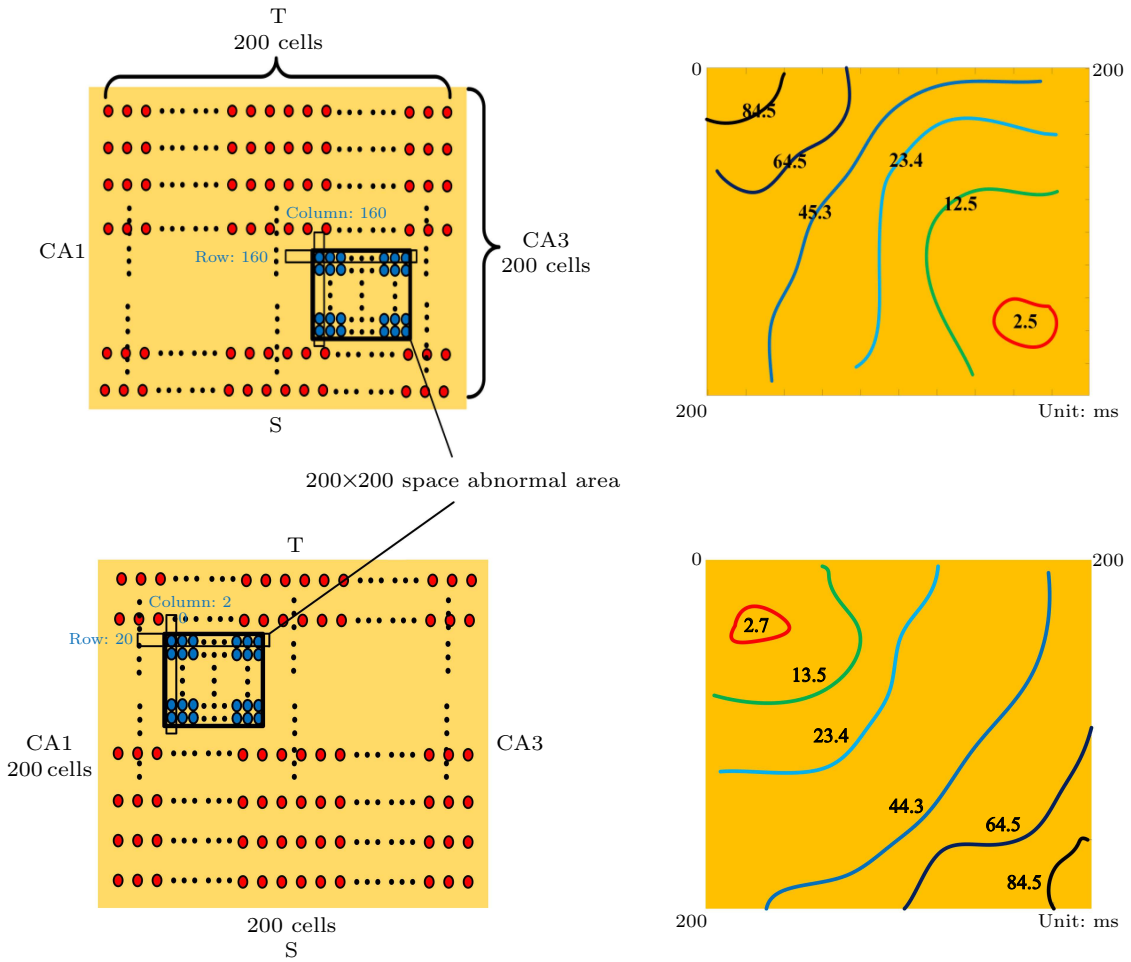


Fig. 20. Effect of cell isomerism in hippocampus on slow wave generation. When the cell spacing decreases to a certain extent, slow-wave sources tend to be generated on the isomeric side rather than the initial stimulation side.

It is observed that the neuronal firing spikes gradually decreases. Eventually, when the applied electric field strength reaches 10 mV/mm, neuronal excitation ceases (see Fig. 19). After a minimal applied electric field is applied, the neuronal pulse disappears completely, and the fast wave spikes of NMDA channels disappear with the slow waves of calcium channels. The transmembrane potential of the neuron fluctuates in the form of a square wave.

3.6. Influence of cell intercellular spacing on slow oscillations

Studies have shown that epileptic-like production is related to the heterogeneity of nerve cells in the brains of human with epilepsy.[30] Related experiments were carried out in the established model to test this conjecture. A 20×20 neuronal region in the neuronal array was selected for the experiment. The spacing of neurons (d_{cc}) within this region was reduced and the spacing of the rest of the region was kept constant (see Fig. 20).

A below-threshold stimulus was applied to the opposite side of the neuronal array and gradually increased until neural excitation was generated in the neuronal array. Neuronal arrays do not produce propagation of neural excitation when external stimuli are less than half the normal value. Slow wave propagation was found in the neuronal array when the external stimulus continued to increase to 0.6 times (-10 mV). Comparison with the experimental phenomenon of normal neuronal arrays leads to the conclusion that abnormal spacing of neurons affects the electric field conduction of neuronal arrays in the hippocampus and induces the generation of abnormal slow waves. In order to better judge the direction of propagation of the wave, we selected the direction of movement of the slow wave peak to study. The peak of the slow wave in previous studies was found to be higher than the fast spike, and the membrane potential peak could reach 0 V. For this wave source, an isochrone plot was constructed. The direction of slow-wave conduction can be seen as septal isomerism to the temporal lobe by the difference in time to peak arrival at 0 V[31]. It can be found by the neuronal potential thermogram that the slow waves are first generated in the neuron-dense area toward the area of normal neuronal spacing.

4. Conclusion

Hippocampal traveling wave oscillations are observed in the hippocampal cortex and are associated with brain activity. *In vitro* experiments suggest that these oscillations rely on electric field coupling between neurons, involving calcium and NMDA channels. However, the exact roles of these channels are not fully understood. Simulations in silicon models can provide a useful alternative to *in vitro* experiments.

Our model consists of a 200×200 neuron array and focuses on ephaptic coupling in the hippocampus. It accurately reproduces the bidirectional propagation of slow waves observed in previous studies. By applying virtual electrodes, we can separate fast- and slow-wave data. The model's reliability is confirmed by comparing wave characteristics with *in vitro* data.

Modulating ion channel conductance in the model reveals that NMDA channels are involved in fast-wave generation, while calcium channels play a key role in slow-wave formation and conduction. Calcium channels influence NMDA channel activity and are crucial for slow periodic oscillations.

Experiments on the model demonstrate that slow-wave conduction can occur even when the neuron array is physically severed, indicating the involvement of electric field conduction. Increasing the gap distance disrupts the propagation of slow waves. Simulations of neural arrays with abnormal neuron spacing reveal that dendritic oscillations can spontaneously occur without external stimulation, shedding light on potential triggers for neurological disorders such as epilepsy.

In summary, our silicon model provides insights into the mechanisms of hippocampal traveling wave oscillations in the hippocampus and confirms the importance of electric field coupling, calcium channels, and NMDA channels in these processes. The findings of this study will provide a valuable reference and foundation for further research on hippocampal wave propagation. In future studies, we plan to refine the model used in this paper by considering factors such as model scale and neuron models. This will enable us to conduct more comprehensive investigations into hippocampal wave propagation and its underlying mechanisms. By improving the model, we aim to gain a deeper understanding of the dynamics and functional significance of hippocampal waves, which will contribute to the broader field of neuroscience.[32]

Acknowledgments

This work was supported in part by the National Natural Science Foundation of China (Grant Nos. 62171312 and 61771330) and the Tianjin Municipal Education Commission Scientific Research Project (Grant No. 2020KJ114).

References

[1] Dehnavi F, Koo-Poeggel P C, Ghorbani M and Marshall L 2021 *Sleep* **44** zsab127
[2] Helfrich R F, Lendner J D, Mander B A, *et al.* 2019 *Nat. Commun.* **10** 3572
[3] Gloveli T, Dugladze T, Rotstein H G, Traub R D, Monyer H, Heinemann U, Whittington M A and Kopell N J 2005 *Proc. Natl. Acad. Sci. USA* **102** 067901
[4] Eliasmith C, Stewart T C, Choo X, Bekolay T, DeWolf T, Tang C and Rasmussen D 2022 *Science* **338** 1202
[5] Faber D S and Korn H 1989 *Physiol. Rev.* **338** 1202

[6] Antic S D, Zhou W, Moore A R, Short S M and Ikonomu K D 2010 *J. Neurosci. Res.* **88** 080201
[7] Rozental R, Andrade-Rozental A F, Zheng X, Urban M, Spray D C and Chiu F C 2001 *Dev. Neurosci.* **23** 056302
[8] Qiu C, Shivacharan R S, Zhang M M and Durand D M 2022 *J. Neurosci.* **35** 040706
[9] Remme M W H, Lengyel M and Gutkin B S 2009 *PLoS Comput. Biol.* **5** e1000493
[10] Zhang M M, Shivacharan R S, Chiang C C, Gonzalez-Reyes L E and Durand D M 2016 *J. Neurosci.* **36** 118104
[11] Chiang C C, Shivacharan R S, Wei X L, Gonzalez-Reyes L E and Durand D M 2016 *J. Physiol.-London* **597** 118104
[12] Chiang C C, Wei X L, Ananthakrishnan A K, Shivacharan R S, Gonzalez-Reyes L E, Zhang M M and Durand D M 2018 *Sci. Rep.* **8** 118104
[13] Diba K 2021 *Neuron* **109** 3071
[14] Magee J C 1998 *J. Neurosci.* **18** 7613
[15] Warman E N, Grill W M and Durand D 1992 *IEEE Trans. Biomed. Eng.* **39** 1244
[16] Swietlik D, Bialowas J, Morys J, Klejbor I and Kusiak A 2019 *Molecules* **24** 118104
[17] Swietlik D, Bialowas J, Morys J, Klejbor I and Kusiak A 2019 *Entropy* **21** 118104
[18] Ghori, Muhammad B, Kang Y and Chen Y Q 2022 *J. Comput. Neurosci.* **50** 040706
[19] Cutsuridis, Vassilis and Wennekers T 2016 *Neural Netw.* **22** 118104
[20] Shivacharan R S, Chiang C C, Zhang M M, Gonzalez-Reyes L E and Durand D M 2019 *Exp. Neurol.* **317** 118104
[21] Bertolino A, Rubino V, Sarnbataro F, Blasi G, Latorre V, Fazio L and Caforio 2016 *Biol. Psychiatry* **60** 118104
[22] Depannemaecker D, Canton S, Luiz E, Rodrigues A M, Scorza C A, Scorza F A and de Almeida A G 2020 *Neural Netw.* **122** 118104
[23] Shivacharan R S, Chiang C C, Wei X L, Subramanian M, Couturier N H, PakalapatiN and Durand D M 2021 *Epilepsia* **62** 118104
[24] Martinet L E, Fiddyment G, Madsen J R and Eskandar E N 2016 *Nat. Commun.* **8** 118104
[25] Lian J, Bikson M, Shuai J and Durand D M 2001 *J. Physiol.-London* **537** 118104
[26] Kibler A B and Durand D M 2011 *Epilepsia* **52** 118104
[27] Colgin L L 2016 *Nat. Rev. Neurosci.* **17** 118104
[28] Schiller J, Major G, Koester H J and Schiller Y 2000 *Nature* **404** 118104
[29] Buzsaki G 2005 *Hippocampus* **15** 118104
[30] Cole S R and Voytek B 2017 *Trends Cogn. Sci.* **21** 118104
[31] Saleh M, Reimer J, Penn R, Ojakangas C L and Hatsopoulos N G 2010 *Neuron* **65** 118104
[32] Choksi B, Mozafari M, VanRullen R and Reddy L 2022 *Neural Netw.* **154** 118104